doi.org/10.36721/PJPS.2026.39.12.335.1

MiR-326 targets ETS1 to activate PI3K/Akt signaling and promote malignant phenotypes in gastric cancer cells

Kai Liang, Xiangyu Zhang and Yin Yang*
Department of General Surgery, Sir Run Run Shaw Hospital, School of Medicine, Zhejiang University, Hangzhou, Zhejiang, 310016, China

Abstract: **Background**: Gastric cancer (GC) remains a leading cause of cancer-related mortality worldwide and effective therapeutic targets remain limited. **Objectives**: This study aimed to investigate the expression and functional role of miR-326 in gastric cancer, identify its direct target gene and elucidate the underlying molecular mechanisms involving the PI3K/Akt signaling pathway and the regulation of inflammatory cytokines. **Methods**: miR-326 expression was detected by qRT-PCR in 56 paired GC tissues and adjacent normal tissues, as well as in GC cell lines (SGC-7901, MKN-45, AGS) and normal GES-1 cells. CCK-8 assays, flow cytometry, Transwell migration/invasion assays and ELISA were performed to assess cell proliferation, apoptosis, migration/invasion and cytokine secretion. Dual-luciferase reporter assay and Western blotting were used to validate the target gene and pathway activation. **Results**: miR-326 was significantly upregulated in GC tissues and cell lines. ETS1 was identified as a direct target of miR-326. Overexpression of miR-326 reduced ETS1 expression, activated the PI3K/Akt pathway (increased p-PI3K and p-AKT), promoted cell proliferation, migration and invasion, inhibited apoptosis and induced an imbalance of inflammatory cytokines (increased IL-6 and TNF-α; decreased IL-10 and IL-17). Co-overexpression of ETS1 or treatment with the PI3K inhibitor LY294002 reversed these effects. **Conclusions**: miR-326 promotes malignant phenotypes in gastric cancer cells by targeting ETS1, activating the PI3K/Akt signaling pathway, and inducing dysregulation of inflammatory cytokines. The miR-326/ETS1/PI3K/Akt axis may serve as a potential diagnostic biomarker and therapeutic target for gastric cancer.

Keywords: ETS1; Gastric cancer; Inflammation; miR-326; Migration; PI3K/Akt pathway; Proliferation

Submitted on 09-01-2026 – Revised on 26-05-2026 – Accepted on 15-06-2026

INTRODUCTION

Gastric cancer is one of the common malignant tumors worldwide, with its incidence and mortality rates ranking fifth among all malignant tumors (Bataga *et al*., 2026). The 5-year survival rate for patients with early-stage gastric cancer can reach 90% to 100%. However, for advanced-stage gastric cancer, even with active comprehensive treatment, the 5-year survival rate remains below 30%. (Yang *et al*., 2023). Therefore, identifying and clarifying new therapeutic targets for GC is of great importance.

MicroRNAs (miRNAs) are a class of endogenous non-coding RNAs with a length of approximately 18 to 22 nucleotides. They mainly exert negative regulation of target gene expression at the post-transcriptional level by binding to the 3' untranslated region (3'UTR) of the target gene mRNA, inhibiting mRNA translation or promoting its degradation (Li *et al*., 2024). Previous studies have shown (Ji C, Han *et al*., 2023) that miRNAs play an important role in tumor development and can act as oncogenes or tumor suppressors in various biological processes, including cell proliferation, apoptosis, migration, invasion, and inflammatory responses.

miR-326 is one of the tumor-related miRNAs that have attracted attention in recent years. Studies have shown that miR-326 is expressed at higher levels in the serum or plasma of patients with various solid tumors and hematological malignancies. In non-small cell lung cancer, miR-326 promotes cell proliferation and inhibits cell apoptosis by regulating the post-transcriptional SNHG12/SLC7A11 axis (Liu *et al*., 2025); in colorectal cancer, miR-326 promotes tumor progression by targeting TGFBR2 (Farc *et al*., 2024). Research on miR-326 in gastric cancer is relatively limited. Relevant studies (Ma *et al*., 2022) have reported that compared with normal gastric mucosal epithelial cells GES-1, miR-326 is expressed at higher levels in gastric cancer cell lines such as AGS, MKN7 and HGC-27 and its upregulation is associated with gastric cancer metastasis and epithelial-mesenchymal transition. However, the specific molecular mechanism of miR-326 in gastric cancer, its downstream target genes, and its association with inflammatory signaling pathways remain to be further elucidated.

ETS1 (E26 transformation-specific sequence 1) is a member of the ETS transcription factor family and plays a significant role in various physiological and pathological processes. Studies have shown that ETS1 is a negative regulator of Th17 cell differentiation, inhibiting Th17 cell maturation and IL-17 production (Wang *et al*., 2025a). In the tumor microenvironment, ETS1 participates in regulating inflammatory responses and immune

**Corresponding author:* e-mail: 3196018@zju.edu.cn

infiltration. However, the expression level of ETS1 in gastric cancer and its regulatory relationship with miR-326 have not been reported.

Bioinformatics prediction (TargetScan, miRDB) revealed that the 3'UTR of ETS1 contains potential binding sites for miR-326, suggesting that ETS1 may be a direct target gene of miR-326. (Nafari *et al*., 2022). Additionally, the PI3K/Akt signaling pathway is one of the core pathways regulating cell proliferation, apoptosis and inflammatory responses and it is often abnormally activated in gastric cancer (Mu *et al*., 2026). Previous studies have shown that the activation of the PI3K/Akt pathway plays an important role in Th17 cell-mediated inflammatory responses (Wang *et al*., 2026). Based on this, it was hypothesized that miR-326 may activate the PI3K/Akt pathway by targeting ETS1, thereby inducing inflammatory responses and promoting the proliferation, migration and invasion of gastric cancer cells.

This study aims to investigate the expression levels of miR-326 in gastric cancer tissues and plasma, to verify whether ETS1 is a direct target gene of miR-326, to clarify the regulatory role of the miR-326/ETS1 axis on the PI3K/Akt signaling pathway and inflammatory response and to evaluate its functional significance in the malignant phenotype of gastric cancer cells, with the expectation of providing new potential targets for the diagnosis and treatment of gastric cancer. Understanding the underlying mechanisms and identifying new therapeutic targets is of great significance.

MATERIALS AND METHODS

Clinical samples

As all tissue samples were obtained from Sir Run Run Shaw Hospital the laboratory tissue bank and de-identified, the ethics committee waived the requirement for individual informed consent. All gastric adenocarcinoma tissues and paired adjacent normal tissues (distance from the tumor edge > 5 cm) were sourced from the laboratory tissue bank.

The gastric cancer tissues and adjacent tissues after surgical resection were immediately washed with sterile normal saline, aliquoted, rapidly frozen in liquid nitrogen, and then transferred to a -80°C refrigerator for long-term storage.

Cell culture

Human gastric cancer cell lines SGC-7901, MKN-45 and AGS were all purchased from the Shanghai Cell Bank of the Chinese Academy of Sciences. The normal gastric mucosal epithelial cell line GES-1 was purchased from the Typical Culture Collection Center (ATCC) in the United States. All cells were cultured in RPMI-1640 medium containing 10% fetal bovine serum (FBS, Gibco, USA) and 1% penicillin-streptomycin (100 U/mL, Gibco) (GES-1 used DMEM high glucose medium). The cells were cultured in a saturated humidity incubator at 37°C and 5% CO_2. Cells were passaged every 2 to 3 days and those in the logarithmic growth phase were used for experiments. All cell lines were regularly tested for mycoplasma and the results were all negative.

Plasmid transfection

miR-326 mimics, negative control mimics (NC mimic), miR-326 inhibitors (anti-miR-326) and negative control inhibitors (anti-NC) were designed and chemically synthesized by Guangzhou Ribo Biotechnology Co., Ltd. The ETS1 overexpression plasmid (pcDNA3.1-ETS1) and the empty vector control (pcDNA3.1-empty) were constructed by Shanghai Jike Gene Chemical Technology Co., Ltd.

24 hours before transfection, logarithmic growth-phase SGC-7901 cells were seeded in 6-well plates (2.5×10^5 cells/well) or 96-well plates (5×10^3 cells/well) to achieve a cell fusion rate of 60-70% during transfection. The transfection was performed using Lipofectamine 3000 transfection reagent (Invitrogen, USA) according to the instructions: miRNA mimics/inhibitors transfection: both at a final concentration of 50 nM; plasmid transfection: 2.5 μg of plasmid per well; co-transfection: miR-326 mimic (50 nM) and ETS1 overexpression plasmid (2.5 μg) were added simultaneously. After 6 hours of transfection, the medium was changed to complete medium, and the cells were cultured for an additional 48 hours. The cells were then collected for subsequent experiments.

Total RNA extraction and real-time quantitative PCR (qRT-PCR)

RNA extraction

Extract total RNA from cells or tissues using TRIzol™ reagent (Invitrogen, USA). Determine the RNA concentration and purity (A260/A280 ratio between 1.8 and 2.0) using a NanoDrop 2000 spectrophotometer (Thermo Fisher, USA).

Reverse transcription

mRNA reverse transcription: Use PrimeScript™ RT Master Mix (TaKaRa, Japan) to reverse transcribe 1 μg of total RNA. miRNA reverse transcription: Use the miRNA First Strand Synthesis Kit (stem-loop method, Guangzhou Ribo Biotechnology Co., Ltd.) for reverse transcription, with a total RNA dosage of 500 ng.

qPCR reaction

Amplification was performed using SYBR® Green Premix Ex Taq™ II (TaKaRa, Japan) on the ABI 7500 real-time fluorescence quantitative PCR system (Applied Biosystems, USA). The reaction conditions were as follows: 95°C for 30 seconds for pre-denaturation; 95°C for 5 seconds for denaturation, 60°C for 34 seconds for annealing and extension, for a total of 40 cycles; then a melting curve analysis was conducted.

Internal participation and relative quantification

miRNA reference: U6 snRNA; mRNA reference: GAPDH. Three technical replicates were set for each sample. The relative expression levels were calculated using the $2^{-}\Delta\Delta Ct$ method (Kadioglu *et al*., 2024). The specificity of the primers was verified by melting curve and agarose gel electrophoresis, and the amplification efficiency was between 90% and 110%. The primer sequences are shown in table 1.

Western blot analysis

Protein extraction

The cells were lysed with RIPA lysis buffer (Biyuntian, China), which contains protease inhibitor (PMSF, 1 mM) and phosphatase inhibitor (PhosSTOP, Roche), on ice for 30 minutes. The mixture was then centrifuged at 12,000 × g for 15 minutes at 4°C to collect the supernatant.

Protein quantification and electrophoresis

The protein concentration was determined using the BCA protein quantitative kit (Thermo Fisher, USA). Equal amounts of protein (30 μg per well) were subjected to SDS-PAGE gel electrophoresis (10% separating gel) and then transferred to a PVDF membrane (Millipore, USA) (Xiao *et al*., 2024).

Incubation with antibodies

Incubate the membrane at room temperature in 5% skim milk - TBST solution for 1 hour. Incubate the membrane with the following primary antibodies at 4°C overnight: anti-ETS1 (1:1000, CST, #14069); anti-p-PI3K (Tyr607, 1:1000, CST, #17366); anti-PI3K (1:1000, CST, #4249); anti-p-AKT (Ser473, 1:2000, CST, #4060); anti-AKT (1:1000, CST, #4691); anti-GAPDH (1:5000, Abcam, #ab9485, used as loading control). The next day, wash the membrane 3 times with TBST, then incubate it at room temperature with an HRP-labeled secondary antibody (1:5000, CST) for 1 hour.

Development and quantification

The ECL reagent (Millipore, USA) was used for developing and the images were captured using the ChemiDoc™ imaging system (Bio-Rad, USA). The band gray values were analyzed using ImageJ. The relative expression level of the target protein = (gray value of the target protein) / (gray value of GAPDH); the relative level of phosphorylated protein = (gray value of the phosphorylated protein) / (gray value of total protein).

Dual luciferase reporter gene assay

The wild-type (WT) or point-mutated (MUT) ETS1 3'UTR sequences were cloned into the pmirGLO dual-luciferase reporter plasmid (Promega, USA). HEK-293T cells were seeded in 24-well plates and co-transfected using Lipofectamine 3000: negative control group: WT-ETS1-3'UTR + NC mimic; experimental group: WT-ETS1-3'UTR + miR-326 mimic; mutant control group: MUT-ETS1-3'UTR + miR-326 mimic. Each group was co-transfected with the pRL-TK kidney luciferase reporter plasmid (Promega, USA) as a reference. After 48 hours of transfection, the luciferase activity was detected using the dual-luciferase reporter gene assay kit (Promega, USA) (Wang *et al*., 2024a). Relative luciferase activity = Firefly luciferase value / Renilla luciferase value. Three replicates were set for each group and the experiment was independently repeated three times.

ELISA assay for cytokine secretion

Collect the cell culture supernatant 48 hours after transfection and centrifuge at 1,000 × g for 10 minutes at 4°C. Use the human IL-6, IL-10, IL-17 and TNF-α ELISA kits (R&D Systems, USA) according to the instructions. Each kit uses standard substances to prepare standard curves (6-8 concentration points, four-parameter logistic fitting, $R^2 > 0.99$). Each sample has 3 replicates. Read the OD at 450 nm on a microplate reader (Bio-Rad, USA) and calculate the cytokine concentration (pg/mL) using the standard curves.

Cell proliferation assay (CCK-8)

SGC-7901 cell proliferation experiment

Transfected SGC-7901 cells were seeded at a density of 5×10^3 cells per well in a 96-well plate, with 5 replicate wells in each group. At 0, 24, 48, and 72 hours after culturing, 10 μL of CCK-8 solution (Dojindo, Japan) was added to each well, and the OD at 450 nm was measured after incubation for 2 hours (Wang *et al*., 2022).

Verification experiment on cell proliferation of MKN-45 and AGS cells

The above proliferation experiments were repeated in the MKN-45 and AGS cell lines. The MKN-45 and AGS cells transfected with miR-326 mimic, NC mimic, anti-miR-326, and anti-NC were inoculated at a density of 5×10^3 cells per well in a 96-well plate, with 5 replicate wells per group. After culturing for 0, 24, 48 and 72 hours, 10 μL of CCK-8 solution (Dojindo, Japan) was added to each well and incubated for 2 hours to measure the OD value at 450 nm. Each cell line's experiment was independently repeated 3 times.

Apoptosis detection (Flow cytometry)

Collect the cells 48 hours after transfection and stain them using the Annexin V-FITC/PI apoptosis detection kit (Beijing Sizheng Bai, China). Set the gating strategy (Miao *et al*., 2023): First, circle the main population of cells in the FSC-SSC scatter plot and exclude debris; then exclude cell aggregates by FSC-A/FSC-H; finally, analyze the apoptosis rate on the FITC/PE dual-parameter scatter plot.

Table 1: Sequences of primers used for qRT-PCR.

GENE	Forward primer (5'→3')	Reverse primer (5'→3')
GAPDH	GGAGCGAGATCCCTCCAAAAT	GGCTGTTGTCATACTTCTCATGG
miR-326	CTCTCTGGGCCCTTCCTCCAG	Universal reverse primer (provided by kit)
ETS-1	GCCTGGATATGCCTGTGAGA	GCCTGGATATGCCTGTGAGA
U6(snRNA)	CTCGCTTCGGCAGCACA	AACGCTTCACGAATTTGCGT

A total of 10,000 events were collected per sample and analyzed with FlowJo v10. The total apoptosis rate = early apoptosis rate (Annexin V+/PI-) + late apoptosis rate (Annexin V+/PI+).

Cell migration and invasion experiment

SGC-7901 cell migration and invasion experiment

Invasion experiment: The upper chamber of the Transwell chamber (8 μm pore size, Corning, USA) was pre-coated with Matrigel matrix gel (diluted 1:8, Corning, USA) and incubated at 37°C for 30 minutes to solidify (Yu *et al*., 2024).

Migration experiment: No Matrigel coating was required. The transfected cells were starved in serum-free medium for 12 hours, resuspended and seeded at 2×10^5 cells per well in the upper chamber of the Transwell. The lower chamber was filled with 600 μL of complete medium containing 20% FBS. After 24 hours of culture, the cells that did not migrate or invade into the upper chamber were removed, fixed with 4% paraformaldehyde, and stained with 0.1% crystal violet. Randomly select 5 200x fields for counting. Each group had 3 replicate wells and the experiment was independently repeated 3 times.

Verification experiment of cell migration in MKN-45 and AGS cells

The above migration experiment was repeated in the MKN-45 and AGS cell lines (no need to coat with Matrigel). The transfected MKN-45 and AGS cells were starved in serum-free medium for 12 hours, resuspended and seeded at 2×10^5 cells per well in the upper chamber of Transwell. The lower chamber was filled with 600 μL of complete medium containing 20% FBS. After 24 hours of culture, the cells that did not migrate into the upper chamber were removed, fixed with 4% paraformaldehyde, and stained with 0.1% crystal violet. The cells in 5 random 200x fields were counted under a microscope. Each cell line's experiment had 3 replicates and was independently repeated 3 times.

PI3K/Akt pathway inhibition experiment

Inhibitor

A pathway-blocking experiment was conducted using the specific PI3K inhibitor LY294002 (catalog number: S9901, Selleck Chemicals, USA) (Hou *et al*., 2024). LY294002 was dissolved in dimethyl sulfoxide (DMSO, Sigma-Aldrich, USA) and prepared as a 50 mM stock solution, which was stored at -20°C in the dark. The working concentration was determined based on the results of the preliminary experiments to be 20 μM.

Experimental group division

The transfected SGC-7901 cells were divided into the following treatment groups: NC mimic + DMSO group: Transfect with NC mimic and add an equal volume of DMSO (final concentration ≤ 0.1%); miR-326 mimic + DMSO group: Transfect with miR-326 mimic and add an equal volume of DMSO; miR-326 mimic + LY294002 group: Transfect with miR-326 mimic and add 20 μM LY294002; NC mimic + LY294002 group: Transfect with NC mimic and add 20 μM LY294002.

Treatment plan

Short-term treatment (to detect phosphorylation levels): 48 hours after transfection, it was switched to fresh complete medium containing LY294002 (20 μM) or an equal volume of DMSO, culturing continued for 2 hours, then the cells were collected for Western Blotting to detect p-PI3K and p-AKT.

Long-term processing (for detecting functional phenotypes): 24 hours after transfection, it was switched to fresh complete medium containing LY294002 (20 μM) or an equal volume of DMSO and culturing was continued for 48 hours before conducting CCK-8 proliferation, flow cytometric apoptosis, Transwell migration/invasion and ELISA assays.

Verification indicators

Pathway inhibition efficiency: By detecting the levels of p-PI3K and p-AKT via Western Blotting, it was confirmed that LY294002 treatment effectively inhibited the phosphorylation and activation of the PI3K/Akt pathway.

Functional phenotype comparison: Differences in cell proliferation, apoptosis, migration/invasion, and inflammatory factor levels between the DMSO control group and the LY294002 treatment group were assessed.

Statistical analysis

All *in vitro cell experiments were independently repeated at least three times,* and the data were presented as mean ± standard deviation (Mean ± SD). Statistical analysis was performed using GraphPad Prism 9.0 software. Comparisons between two groups were conducted using a two-tailed Student's t-test (normal distribution and homogeneity of variance were met), and comparisons

among multiple groups were performed using one-way ANOVA followed by Tukey's post hoc test. For two-factor designs (such as miRNA treatment × inhibitor treatment in the inhibitor experiment), a two-way ANOVA was used, followed by Sidak's post hoc test. A difference was considered statistically significant when $P < 0.05$.

RESULTS

The expression of miR-326 is elevated in gastric cancer tissues and cells.

qRT-PCR results (Fig. 1A) showed that the relative expression level of miR-326 was significantly higher in gastric cancer tissues (4.82 ± 1.36) than in paired adjacent normal tissues (1.02 ± 0.28) ($P < 0.001$, 95% CI: 3.12–4.48).

In gastric cancer cell lines, compared with normal gastric mucosal epithelial cells GES-1 (1.00 ± 0.12), the expression of miR-326 in SGC-7901 cells was approximately 5.6 times higher (5.62 ± 0.94, $P < 0.001$), in MKN-45 cells it was approximately 3.8 times higher (3.82 ± 0.71, $P < 0.01$) and in AGS cells it was approximately 4.3 times higher (4.31 ± 0.85, $P < 0.01$) (Fig. 1B).

ETS1 is a direct target gene of miR-326.

The level of ETS1 mRNA in gastric cancer tissues was significantly lower than that in the paired adjacent normal tissues (0.38 ± 0.11 vs. 1.02 ± 0.24, $P < 0.001$, 95% CI: -0.520 to -0.760) and the expression of miR-326 was significantly negatively correlated with the expression of ETS1 mRNA (Pearson *r* = -0.680, $P < 0.001$, Fig. 2A). Western blot analysis further confirmed that the ETS1 protein level in gastric cancer tissues was approximately 58% lower than in adjacent tissues (Fig. 2B, $P < 0.01$).

The results of the dual-luciferase reporter gene assay (Fig. 2C) showed that after co-transfection with miR-326 mimic and the wild-type ETS1 3'UTR reporter plasmid, the relative luciferase activity was significantly reduced by approximately 41% compared to the NC mimic control group (0.59 ± 0.06 vs. 1.00 ± 0.08, $P < 0.001$, 95% CI: -0.52 to -0.30). However, when the ETS1 3'UTR binding site was mutated, there was no significant difference in luciferase activity between the two groups (0.95 ± 0.07 vs. 1.02 ± 0.06, $P = 0.210$).

miR-326 activates the PI3K/Akt pathway by targeting ETS1

After overexpression of miR-326 in SGC-7901 cells, the protein level of ETS1 was reduced by approximately 53% compared to the NC mimic control group ($P < 0.01$), while the level of p-PI3K increased by approximately 2.4 times (2.41 ± 0.31 vs. 1.00 ± 0.12, $P < 0.01$) and the level of p-AKT increased by approximately 2.8 times (2.81 ± 0.35 vs. 1.00 ± 0.11, $P < 0.001$); there were no significant differences in total PI3K and total AKT levels among the groups (Figs. 3A-3B). After transfection with anti-miR-326, the protein level of ETS1 increased by approximately 1.9 times (1.91 ± 0.22 vs. 1.00 ± 0.09, $P < 0.01$) and the levels of p-PI3K and p-AKT decreased by approximately 46% and 52% respectively (Fig. 3C).

After co-transfection with the miR-326 mimic and ETS1 overexpression plasmid, the ETS1 protein level returned to a level comparable to that of the control group (0.92 ± 0.10 vs. 1.00 ± 0.09, $P = 0.38$). The co-overexpression of ETS1 completely reversed the activation of the PI3K/Akt pathway induced by miR-326 mimic: the level of p-PI3K decreased from 2.41 times to 1.12 ± 0.13 ($P = 0.29$) and the level of p-AKT decreased from 2.81 times to 1.08 ± 0.11 ($P = 0.34$) (Fig. 3D).

miR-326 promotes the proliferation of gastric cancer cells and inhibits apoptosis.

CCK-8 proliferation assays showed that the proliferative capacity of SGC-7901 cells significantly increased after transfection with miR-326 mimics. Compared with the NC mimic control group, the OD_{450} value of the miR-326 mimic group increased approximately 2.1 times at 72 hours (2.14 ± 0.18 vs. 1.00 ± 0.09, $P < 0.001$, Fig. 4A). Transfection with anti-miR-326 reduced the cell proliferation ability by approximately 41% (0.59 ± 0.07 vs. 1.00 ± 0.08, $P < 0.01$). The CCK-8 experiments were repeated in MKN-45 and AGS cells and the results were consistent with those of SGC-7901 cells (Fig. 4B-4C).

Flow cytometry apoptosis detection results (Fig. 4D) showed that the total apoptosis rate decreased from 8.2% ± 1.1% to 3.1% ± 0.6% after transfection with the miR-326 mimic (a decrease of approximately 62%; $P < 0.001$). The total apoptosis rate increased to 15.6% ± 1.8% after transfection with anti-miR-326 ($P < 0.001$). After co-transfection with the ETS1 overexpression plasmid, the total apoptosis rate recovered to 6.9% ± 0.9% ($P < 0.01$, Fig. 4C).

miR-326 promotes the migration and invasion of gastric cancer cells

The results of the Transwell migration and invasion assays (Figs. 5A-5B) showed that after transfection with miR-326 mimic, the number of migrating cells in SGC-7901 cells increased approximately 2.4 times (238 ± 21 vs. 100 ± 9, $P < 0.001$) and the number of invasive cells increased approximately 2.2 times (186 ± 17 vs. 100 ± 8, $P < 0.001$). After transfection with anti-miR-326, the number of migrating cells decreased by approximately 54% (46 ± 6 vs. 100 ± 9, $P < 0.01$) and the number of invasive cells decreased by approximately 49% (51 ± 6 vs. 100 ± 8, $P < 0.01$). The Transwell migration experiments were repeated in MKN-45 and AGS cells and the results were consistent with those of SGC-7901 cells (Figs. 5C-5D).

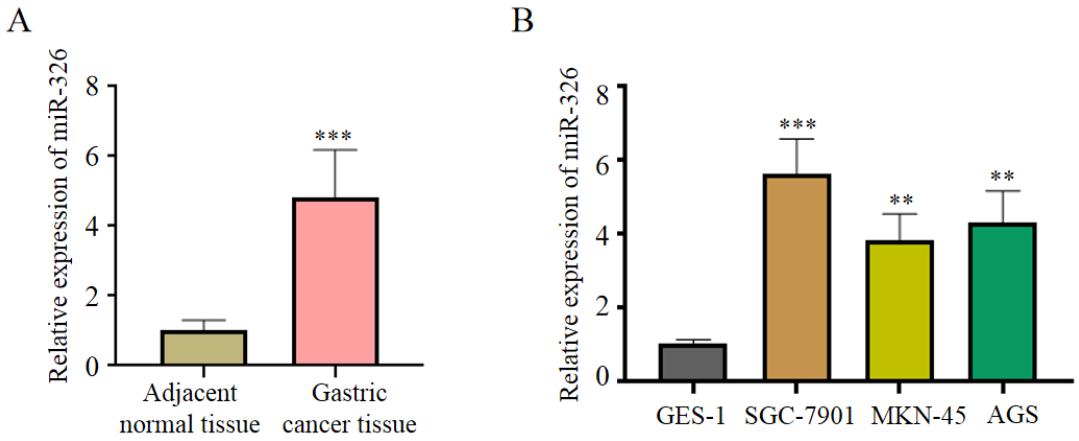

Fig. 1: miR-326 expression is elevated in gastric cancer tissues and cell lines.
(A) Quantitative real-time PCR (qRT-PCR) was performed to detect the expression level of miR-326 in 56 pairs of gastric cancer (GC) tissues and matched adjacent normal (AN) tissues. The expression level was normalized to U6 snRNA, and the relative expression was calculated using the $2^{-}\Delta\Delta Ct$ method. Data are presented as mean ± SD. ()***P < 0.001 versus adjacent normal tissues, paired t-test; (B) qRT-PCR was performed to detect the expression level of miR-326 in GES-1 (normal gastric mucosal epithelial cells), SGC-7901, MKN-45, and AGS gastric cancer cell lines. The expression level was normalized to U6 snRNA and calculated relative to GES-1 cells. Data are presented as mean ± SD, n = 3 independent experiments. **P < 0.01, ***P < 0.001 versus GES-1 cells, one-way ANOVA with Tukey's post-hoc test.

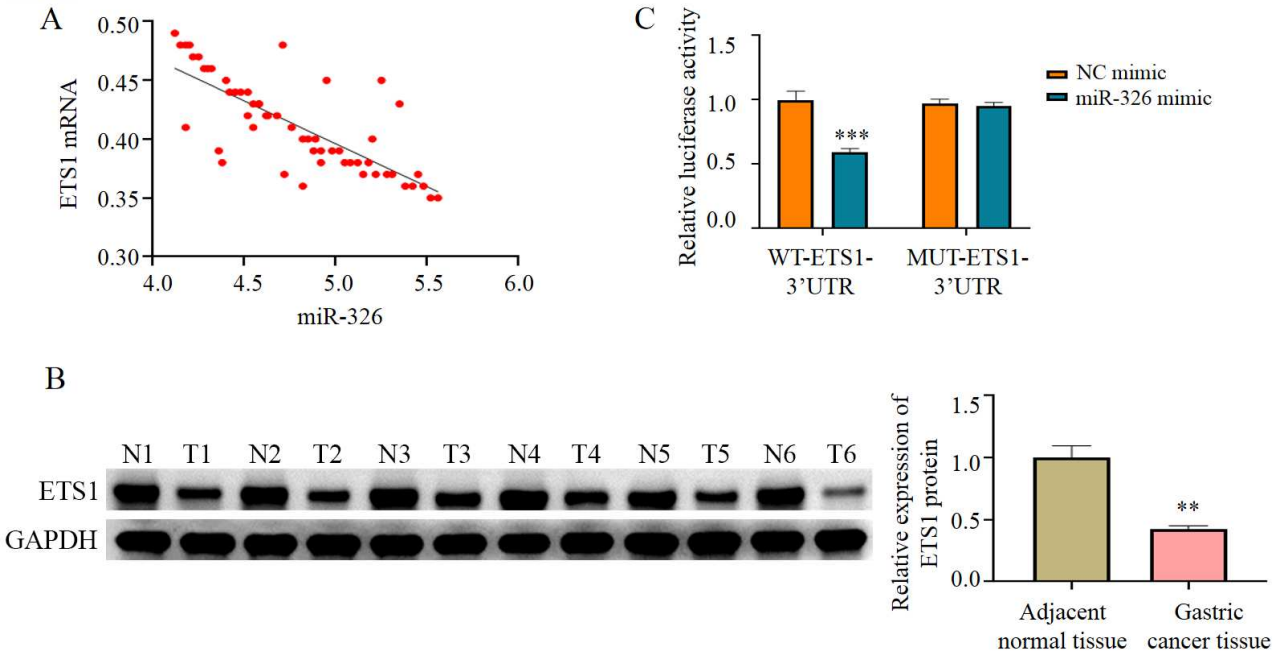

Fig. 2: ETS1 is a direct target gene of miR-326.
Pearson correlation analysis of miR-326 and ETS1 mRNA expression levels in 56 gastric cancer tissues. Each dot represents an individual tissue sample. The correlation coefficient (r) and P value are indicated. ***P < 0.001, Pearson correlation test; (B) Western blot analysis of ETS1 protein expression in 6 pairs of gastric cancer (T1-T6) and matched adjacent normal (N1-N6) tissues. GAPDH was used as a loading control. Representative Western blot images are shown above, and the bar graph below shows the quantitative analysis of ETS1 protein levels normalized to GAPDH. Data are presented as mean ± SD, n = 6 paired samples. **P < 0.01, paired t-test; (C) Dual-luciferase reporter assay the direct binding of miR-326 to the ETS1 3'UTR. HEK-293T cells were co-transfected with wild-type (WT) or mutant (MUT) ETS1 3'UTR reporter plasmids together with NC mimic or miR-326 mimic. Firefly luciferase activity was normalized to Renilla luciferase activity (pRL-TK). Data are presented as mean ± SD, n = 3 independent experiments. ***P < 0.001 vs. WT + NC mimic group, paired t-test.

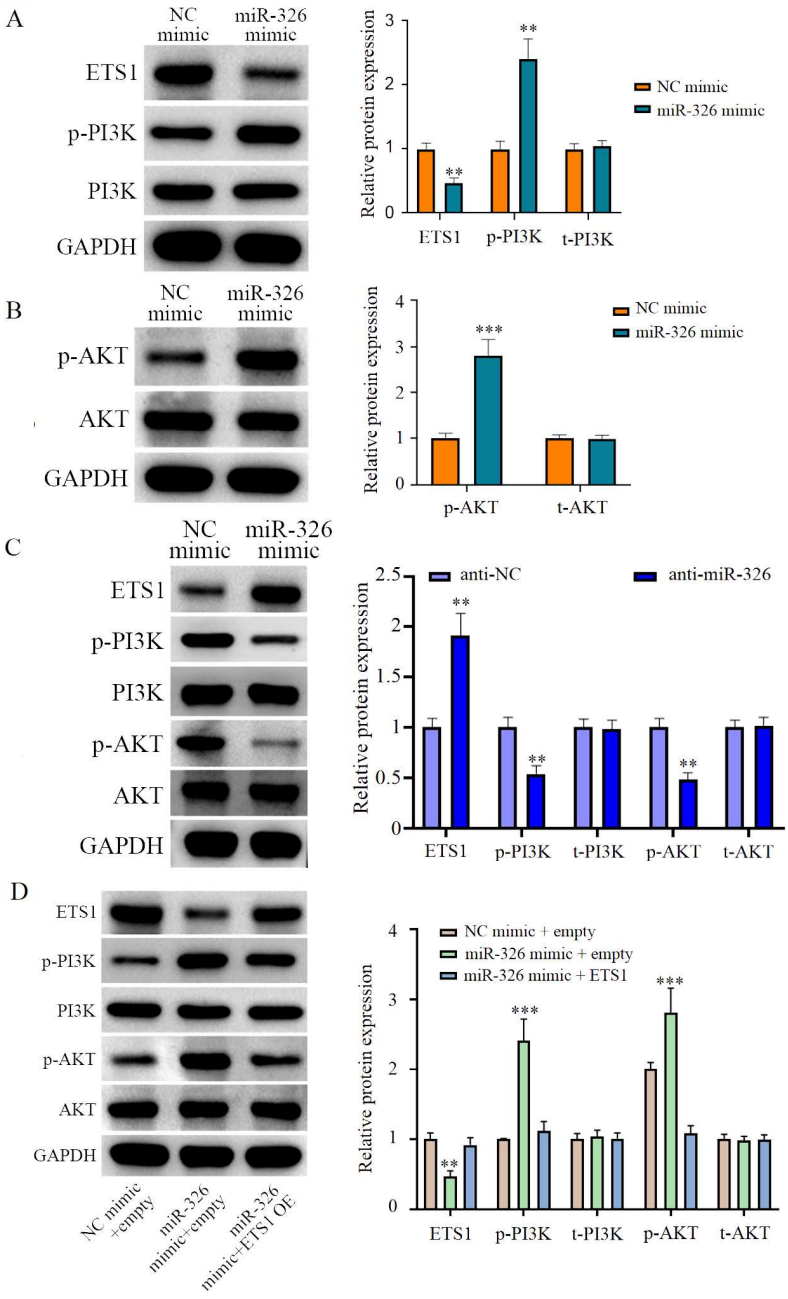

Fig. 3: miR-326 activates the PI3K/Akt pathway by targeting ETS1.
Western blot analysis of ETS1, p-PI3K, total PI3K and GAPDH in SGC-7901 cells transfected with NC mimic or miR-326 mimic. GAPDH served as a loading control. Representative Western blot images are shown above, and the bar graph below shows the quantitative analysis of protein levels normalized to GAPDH. Data are presented as mean ± SD, n = 3 independent experiments. (**P < 0.01 vs. NC mimic group, paired t-test); (B) Western blot analysis of p-AKT, total AKT, and GAPDH in SGC-7901 cells transfected with NC mimic or miR-326 mimic. Representative Western blot images are shown above, and the bar graph below shows the quantitative analysis of protein levels normalized to GAPDH. Data are presented as mean ± SD, n = 3 independent experiments. (***P < 0.001 vs. NC mimic group, paired t-test); (C) Western blot analysis of ETS1, p-PI3K, total PI3K, p-AKT, total AKT and GAPDH in SGC-7901 cells transfected with anti-NC or anti-miR-326. Representative Western blot images are shown above, and the bar graph below shows the quantitative analysis of protein levels normalized to GAPDH. Data are presented as mean ± SD, n = 3 independent experiments. (**P < 0.01 vs. anti-NC group, paired t-test); (D) Western blot analysis of ETS1, p-PI3K, total PI3K(t- PI3K), p-AKT, total AKT(t- AKT), and GAPDH in SGC-7901 cells co-transfected with miR-326 mimic and ETS1 overexpression plasmid (pcDNA3.1-ETS1). NC mimic + empty vector (pcDNA3.1-empty) served as the control group. Representative Western blot images are shown above, and the bar graph below shows the quantitative analysis of protein levels normalized to GAPDH. Data are presented as mean ± SD, n = 3 independent experiments. (**P < 0.01, ***P < 0.001 vs. NC mimic + empty group, two-way ANOVA with Sidak's post-hoc test).

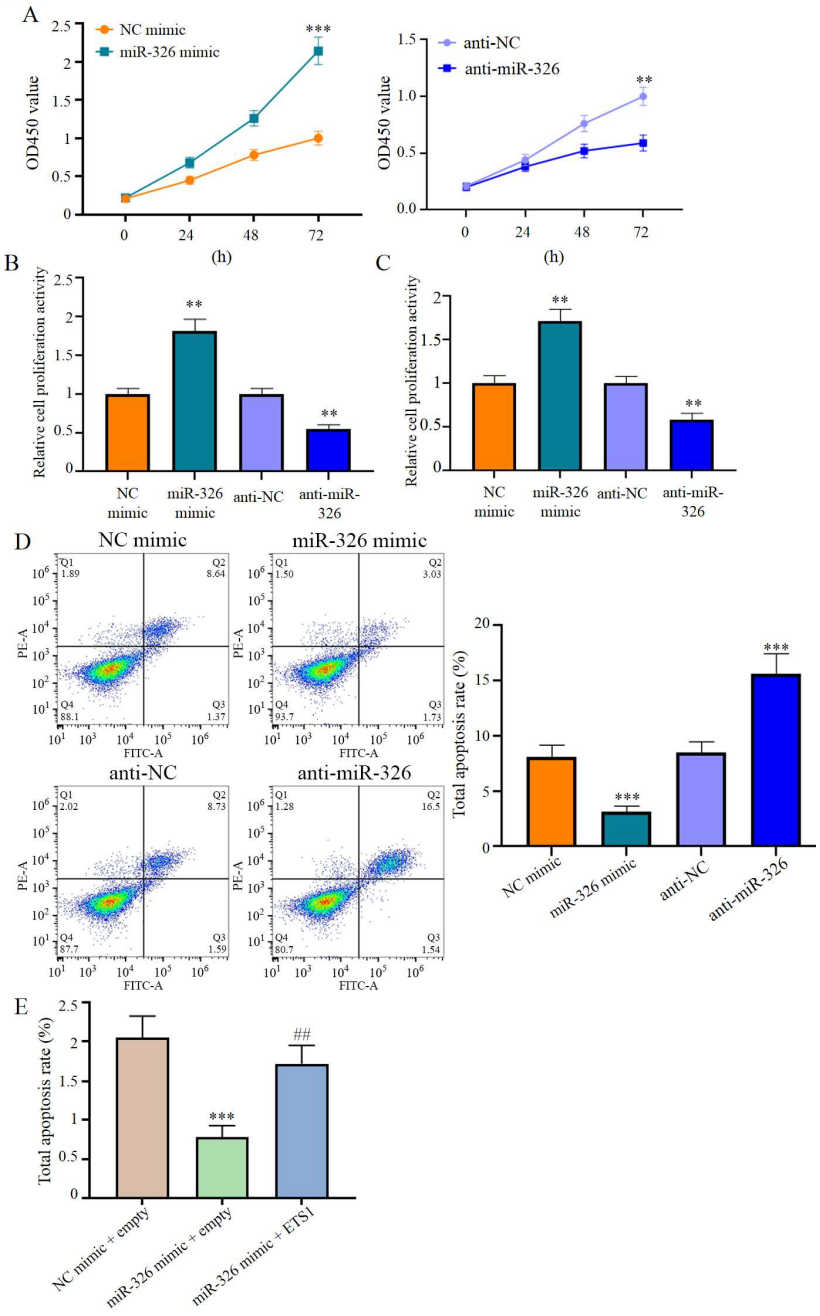

Fig. 4: Effects of miR-326 on proliferation and apoptosis of gastric cancer cells.
CCK-8 assay was performed to evaluate the proliferation of SGC-7901 cells transfected with NC mimic, miR-326 mimic, anti-NC, or anti-miR-326. Cell viability was measured at 0, 24, 48, and 72 hours post-transfection. OD_{450} values are presented as mean ± SD, n = 5 replicates per group, with three independent experiments. (***P < 0.001 vs. NC mimic group; **P < 0.01 vs. anti-NC group, two-way ANOVA.); (B-C) CCK-8 assay was performed to evaluate the proliferation of MKN-45 (B) and AGS (C) cells transfected with NC mimic, miR-326 mimic, anti-NC, or anti-miR-326. Cell viability was measured at 72 hours post-transfection. Data are presented as mean ± SD, n = 5 replicates per group, with three independent experiments. (**P < 0.01 vs. respective control groups, paired t-test.); (D) Flow cytometric analysis of apoptosis in SGC-7901 cells transfected with NC mimic, miR-326 mimic, anti-NC, or anti-miR-326. Cells were stained with Annexin V-FITC and propidium iodide (PI). Representative flow cytometry scatter plots are shown on the left, and the bar graph on the right shows the quantitative analysis of total apoptosis rates (early apoptosis + late apoptosis). Data are presented as mean ± SD, n = 3 independent experiments. (***P < 0.001 vs. respective control groups, paired t-test.); (E) Flow cytometric analysis of apoptosis in SGC-7901 cells co-transfected with miR-326 mimic and ETS1 overexpression plasmid (pcDNA3.1-ETS1). NC mimic + empty vector (pcDNA3.1-empty) served as the control group. Representative flow cytometry scatter plots are shown, and the bar graph shows the quantitative analysis of total apoptosis rates. Data are presented as mean ± SD, n = 3 independent experiments. (***P < 0.001 vs. NC mimic + empty group; ##P < 0.01 vs. miR-326 mimic + empty group, paired t-test.)

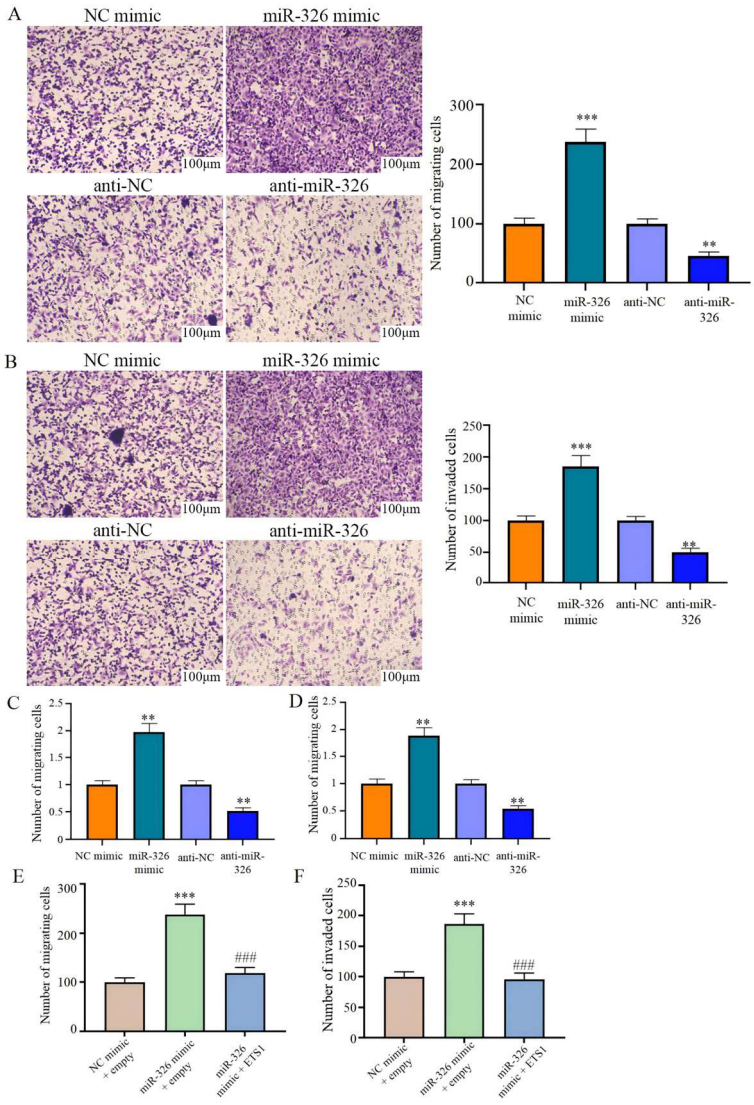

Fig. 5: Effects of miR-326 on migration and invasion of gastric cancer cells.
Transwell migration assay was performed to evaluate the migratory capacity of SGC-7901 cells transfected with NC mimic, miR-326 mimic, anti-NC, or anti-miR-326. Cells that migrated to the lower chamber were fixed with 4% paraformaldehyde, stained with 0.1% crystal violet, and counted under a light microscope at 200× magnification. Representative crystal violet staining images are shown above, and the bar graph below shows the quantitative analysis of migrated cells per field. Data are presented as mean ± SD, n = 3 independent experiments with 3 replicates per group. (***P < 0.001, **P < 0.01 vs. respective control groups, paired t-test.); (B) Transwell invasion assay was performed to evaluate the invasive capacity of SGC-7901 cells transfected with NC mimic, miR-326 mimic, anti-NC, or anti-miR-326. The upper chamber was pre-coated with Matrigel (1:8 dilution) before cell seeding. Cells that invaded through the Matrigel to the lower chamber were fixed, stained with crystal violet and counted under a light microscope at 200× magnification. Representative crystal violet staining images are shown above and the bar graph below shows the quantitative analysis of invaded cells per field. Data are presented as mean ± SD, n = 3 independent experiments with 3 replicates per group. (***P < 0.001, **P < 0.01 vs. respective control groups, paired t-test.); (C-D) Transwell migration assay was performed to evaluate the migratory capacity of MKN-45; (C) and AGS; (D) cells transfected with NC mimic, miR-326 mimic, anti-NC, or anti-miR-326. Cells were counted at 200× magnification. Data are presented as mean ± SD, n = 3 independent experiments with 3 replicates per group. (**P < 0.01 vs. respective control groups, paired t-test.); (E) Transwell migration assay was performed to evaluate the migratory capacity of SGC-7901 cells co-transfected with miR-326 mimic and ETS1 overexpression plasmid (pcDNA3.1-ETS1). NC mimic + empty vector (pcDNA3.1-empty) served as the control group. Data are presented as mean ± SD, n = 3 independent experiments with 3 replicates per group. (***P < 0.001 vs. NC mimic + empty group; ###P < 0.001 vs. miR-326 mimic + empty group, paired t-test.); (F) Transwell invasion assay was performed to evaluate the invasive capacity of SGC-7901 cells co-transfected with miR-326 mimic and ETS1 overexpression plasmid (pcDNA3.1-ETS1). The upper chamber was pre-coated with Matrigel. NC mimic + empty vector served as the control group. Data are presented as mean ± SD, n = 3 independent experiments with 3 replicates per group. (***P < 0.001 vs. NC mimic + empty group; ###P < 0.001 vs. miR-326 mimic + empty group, paired t-test.

After co-transfection with the ETS1 overexpression plasmid, the number of migrating cells decreased from 238 ± 21 to 118 ± 12 ($P < 0.001$) and the number of invasive cells decreased from 186 ± 17 to 96 ± 10 ($P < 0.001$) (Figs. 5E-5F).

miR-326 regulates the secretion of inflammatory factors through ETS1

The ELISA test results (Figs. 6A-6D) showed that after transfection with miR-326 mimic, the levels of pro-inflammatory factors IL-6 (245.6 ± 28.3 pg/mL vs. 100.0 ± 11.2 pg/mL, $P < 0.001$) and TNF-α (187.3 ± 21.5 pg/mL vs. 100.0 ± 10.6 pg/mL, $P < 0.001$) significantly increased, while the levels of anti-inflammatory factors IL-10 (52.3 ± 7.1 pg/mL vs. 100.0 ± 9.8 pg/mL, $P < 0.01$) and IL-17 (55.2 ± 6.8 pg/mL vs. 100.0 ± 9.5 pg/mL, $P < 0.01$) significantly decreased. The opposite trend was observed after transfection with anti-miR-326.

After co-transfection with the ETS1 overexpression plasmid, IL-6 decreased to 138.4 ± 16.2 pg/mL ($P < 0.01$), TNF-α decreased to 112.6 ± 13.5 pg/mL ($P < 0.01$), IL-10 increased to 76.8 ± 8.4 pg/mL ($P < 0.05$) and IL-17 increased to 80.5 ± 9.1 pg/mL ($P < 0.05$) (Figs. 6E-6H).

Inhibiting the PI3K/Akt pathway can reverse the cancer-promoting effect mediated by miR-326

After treating miR-326 mimic-transfected SGC-7901 cells with the PI3K inhibitor LY294002, the Western blot results showed that the level of p-PI3K decreased by approximately 71% (0.29 ± 0.05 vs. 1.00 ± 0.11, $P < 0.001$) and the level of p-AKT decreased by approximately 68% (0.32 ± 0.06 vs. 1.00 ± 0.10, $P < 0.001$) (Fig. 7A).

The functional phenotypic experiments showed (Figs. 7B-7E) that after treatment with LY294002, the 72-hour OD_{450} value decreased from 2.14 ± 0.18 to 1.28 ± 0.12, the total apoptosis rate increased from 3.1% ± 0.6% to 7.5% ± 0.8%, the number of migrating cells decreased from 238 ± 21 to 115 ± 13, the number of invasive cells decreased from 186 ± 17 to 104 ± 11 and the levels of IL-6 and TNF-α decreased by approximately 57% and 61% respectively, while the levels of IL-10 and IL-17 increased by approximately 58% and 53% respectively (all $P < 0.01$). The treatment with LY294002 alone had no significant effect on these phenotypes (all $P > 0.05$).

DISCUSSION

Gastric cancer (GC), which usually originates from gastric mucosal cells, most commonly occurs in individuals between 40 and 70 years of age. Surgery is a potential curative option for GC patients, often combined with perioperative chemotherapy, radiotherapy and targeted biological therapies to achieve extended disease management.(Wang *et al*.,2024b). However, advanced GC still lacks effective treatment; even when it is actively integrated into treatment, its 5-year survival rate is still less than 30% (Janjigian *et al*., 2026). Therefore, it is important to study and clarify new targets for improving the treatment of GC. miRNAs are endogenous short non-coding RNAs approximately 18–22 nucleotides in length and lack protein-coding capacity. A great deal of research has shown that miRNAs play important roles in cancer. (Ye *et al*., 2025; Asensio *et al*., 2025). At present, it has been found that short-chain noncoding RNAs can function and serve as a new indicator of various cancers. A previous study (Shen *et al*., 2024) reported that the miR-326 sequence is highly conserved across vertebrates and may promote cellular senescence and cancer in a tissue-dependent manner. This study found that miR-326 was significantly upregulated in gastric cancer tissues and plasma, and its high expression was associated with enhanced proliferation, migration, and invasion in gastric cancer cells. Using dual luciferase reporter gene assays and Western blot verification, it was confirmed that ETS1 is a direct target of miR-326. Further functional experiments demonstrated that miR-326 targets and inhibits ETS1, thereby activating the PI3K/Akt signaling pathway, promoting the secretion of pro-inflammatory factors and inhibiting the production of anti-inflammatory factors. Using the PI3K-specific inhibitor LY294002 partially reversed the cancer-promoting phenotype and the imbalance in inflammatory factors induced by miR-326 mimics, supporting the notion that the PI3K/Akt pathway plays a key role in the malignant transformation of gastric cancer cells mediated by miR-326.

From a mechanistic perspective, the findings of this study can be summarized into several interrelated levels. The direct targeting regulation of ETS1 by miR-326 is the initiating event of the entire signaling pathway. As a transcription factor, ETS1 has a conserved miR-326 binding site in its 3' UTR. miR-326 inhibits the translation efficiency of ETS1 through the classical miRNA-mRNA interaction mechanism, resulting in a decrease in the protein level of ETS1 (Zhang *et al*., 2022; Jiang *et al*., 2022). Since ETS1 plays an anti-cancer role in various cell types, its downregulation creates conditions for the activation of downstream oncogenic signaling pathways (Wang *et al*., 2025b). Further analysis revealed that the downregulation of ETS1's negative regulation not only inhibits the PI3K/Akt pathway. In this study, a decrease in ETS1 protein levels was significantly negatively correlated with increases in p-PI3K and p-AKT levels. ETS1 may regulate the PI3K/Akt pathway through two mechanisms: first, as a transcription factor, ETS1 may directly regulate the expression of negative regulators of PI3K or Akt (Liu *et al*., 2024); second, ETS1 may indirectly affect the membrane recruitment or activation of PI3K (He *et al*., 2023).

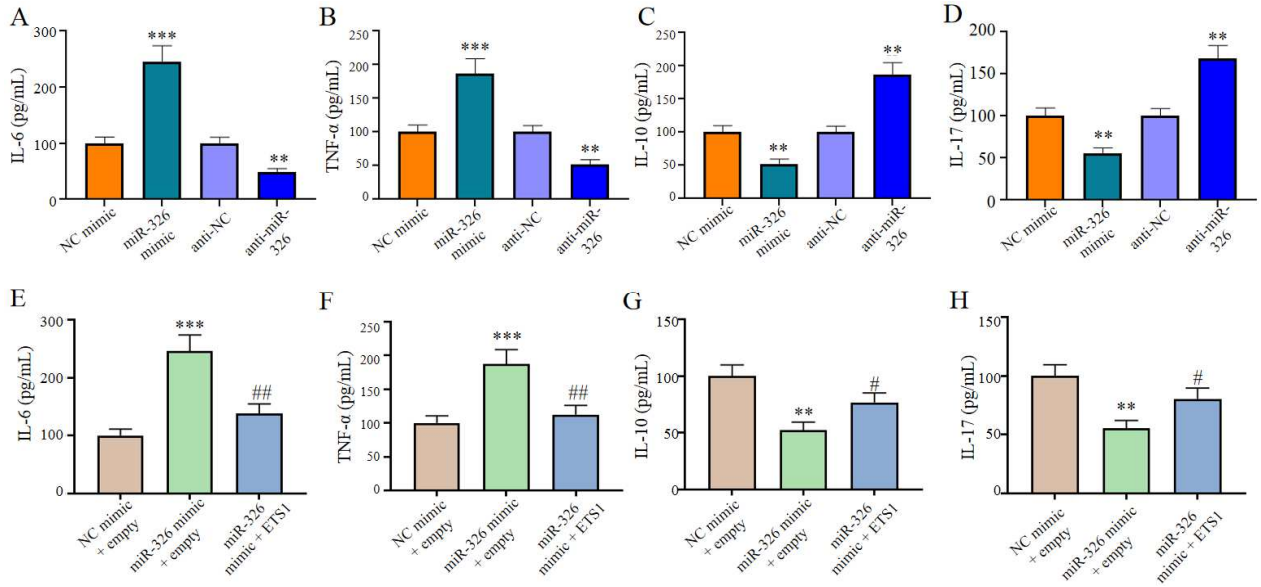

Fig. 6: miR-326 regulates inflammatory cytokine secretion through ETS1.
(A-D) ELISA was performed to detect the concentrations of IL-6 (A), TNF-α; (B) IL-10; (C) and IL-17; (D) in the culture supernatants of SGC-7901 cells transfected with NC mimic, miR-326 mimic, anti-NC, or anti-miR-326. Cell culture supernatants were collected 48 hours post-transfection and centrifuged at 1,000 × g for 10 minutes at 4°C. Cytokine concentrations were measured using commercial ELISA kits according to the manufacturer's instructions. Standard curves were generated using eight standard concentrations with four-parameter logistic regression ($R^2 > 0.99$). Data are presented as mean ± SD, n = 3 independent experiments with 3 replicates per group. (***P < 0.001, **P < 0.01 vs. respective control groups, paired t-test.); (E-H) ELISA was performed to detect the concentrations of IL-6 (E), TNF-α (F), IL-10 (G), and IL-17 (H) in the culture supernatants of SGC-7901 cells co-transfected with miR-326 mimic and ETS1 overexpression plasmid (pcDNA3.1-ETS1). NC mimic + empty vector (pcDNA3.1-empty) served as the control group. Cell culture supernatants were collected 48 hours post-transfection and processed as described above. Data are presented as mean ± SD, n = 3 independent experiments with 3 replicates per group. (***P < 0.001, **P < 0.01 vs. NC mimic + empty group; ##P < 0.01, #P < 0.05 vs. miR-326 mimic + empty group, paired t-test.)

The overexpression of ETS1 in this study completely reverses the PI3K/Akt phosphorylation induced by the miR-326 mimic, suggesting that ETS1 plays a negative regulatory role upstream of the PI3K/Akt pathway. Based on this, the activation of the PI3K/Akt pathway further drives the imbalance of the inflammatory factor network. After Akt kinase activation, it can phosphorylate multiple downstream transcription factors, which directly regulate the transcription of cytokines such as IL-6, TNF-α, IL-10 and IL-17 (Deng *et al*., 2024). The observed increase in pro-inflammatory factors and decrease in anti-inflammatory factors in this study are consistent with the transcriptional profile observed after NF-κB activation. Ultimately, these molecular events converge on changes in cellular functional phenotypes: the enhanced PI3K/Akt signaling promotes cell cycle progression and survival, while the imbalance in inflammatory factors shapes a microenvironment conducive to tumor growth. It should be noted that LY294002 in this study can only partially reverse the proliferation enhancement and apoptosis inhibition induced by the miR-326 mimic, suggesting that, in addition to the PI3K/Akt pathway, the downregulation of ETS1 may also activate parallel signaling pathways involved in regulating the malignant phenotype of gastric cancer cells.

Compared with previous studies, this research established for the first time the regulatory axis of miR-326/ETS1/PI3K/Akt/inflammatory factors in gastric cancer. Previously, it was reported that miR-326 was expressed at an elevated level in gastric cancer cell lines and was associated with epithelial-mesenchymal transition, but its direct target genes were not clearly identified (Qin *et al*., 2022). This study found that ETS1 is a direct target of miR-326, and that ETS1 is expressed at lower levels in gastric cancer tissues and is negatively correlated with miR-326 expression. This finding is consistent with the reports that ETS1 acts as a tumor suppressor in various tumors (Xu *et al*., 2023, Han *et al*., 2024). In colorectal and lung cancers, miR-326 targets TGFBR2 and PDK1, respectively, suggesting that its oncogenic function may be tissue-specific and that the downstream target gene spectrum varies depending on tumor type. It is noteworthy that in colorectal cancer studies, miR-326 affects TGF-β signaling through TGFBR2, whereas the PI3K/Akt pathway identified in this study differs from this, suggesting that miR-326 can act on distinct signaling networks in distinct tumor contexts.

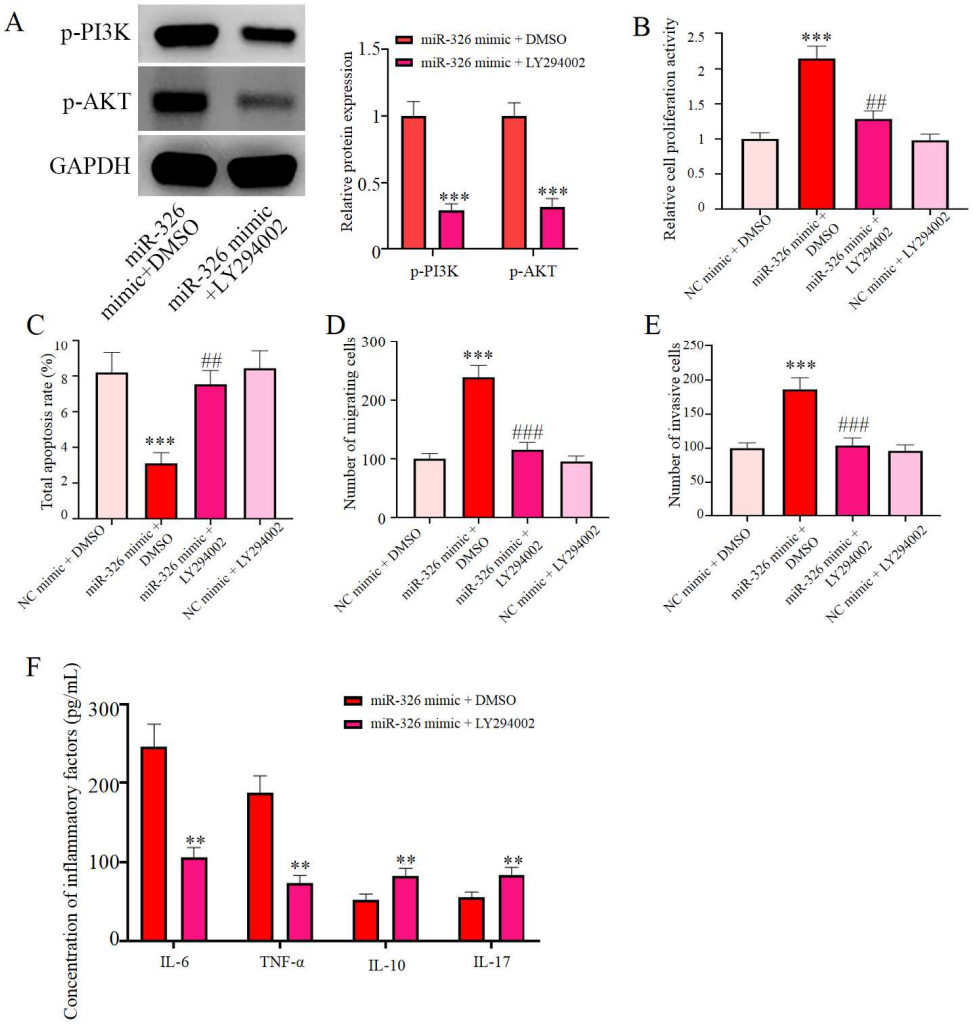

Fig. 7: Inhibition of the PI3K/Akt pathway reverses miR-326-mediated pro-tumorigenic effects.
(A) Western blot analysis of p-PI3K, p-AKT, and GAPDH in SGC-7901 cells transfected with miR-326 mimic and treated with DMSO (vehicle control) or LY294002 (20 μM, specific PI3K inhibitor) for 2 hours. GAPDH served as a loading control. Representative Western blot images are shown above, and the bar graph below shows the quantitative analysis of protein levels normalized to GAPDH. Data are presented as mean ± SD, n = 3 independent experiments. (***P < 0.001 vs. DMSO control group, paired t-test.); (B) CCK-8 assay was performed to evaluate the proliferation of SGC-7901 cells transfected with NC mimic or miR-326 mimic and treated with DMSO or LY294002 (20μM) for 48 hours. Cell viability was measured at 72 hours post-transfection. OD_{450} values are presented as mean ± SD, n = 5 replicates per group, with three independent experiments. (***P < 0.001 vs. NC mimic + DMSO group; ##P < 0.01 vs. miR-326 mimic + DMSO group; two-way ANOVA with Sidak's post-hoc test.); (C) Flow cytometric analysis of apoptosis in SGC-7901 cells transfected with NC mimic or miR-326 mimic and treated with DMSO or LY294002 (20 μM) for 48 hours. Cells were stained with Annexin V-FITC and propidium iodide (PI). Representative flow cytometry scatter plots are shown on the left, and the bar graph on the right shows the quantitative analysis of total apoptosis rates (early apoptosis + late apoptosis). Data are presented as mean ± SD, n = 3 independent experiments. (***P < 0.001 vs. NC mimic + DMSO group; ##P < 0.01 vs. miR-326 mimic + DMSO group, two-way ANOVA with Sidák's post-hoc test.); (D) Transwell migration assay was performed to evaluate the migratory capacity of SGC-7901 cells transfected with NC mimic or miR-326 mimic and treated with DMSO or LY294002 (20 μM) for 48 hours. Migrated cells were stained with crystal violet and counted under a light microscope at 200× magnification. Data are presented as mean V SD, n = 3 independent experiments with 3 replicates per group. (***P < 0.001 vs. NC mimic + DMSO group; ###P < 0.001 vs. miR-326 mimic + DMSO group, two-way ANOVA with Sidák's post-hoc test.); (E) Transwell invasion assay was performed to evaluate the invasive capacity of SGC-7901 cells transfected with NC mimic or miR-326 mimic and treated with DMSO or LY294002 (20 μM) for 48 hours. The upper chamber was pre-coated with Matrigel. Invaded cells were stained with crystal violet and counted under a light microscope at 200× magnification. Data are presented as mean ± SD, n = 3 independent experiments with 3 replicates per group. ()***P < 0.001 vs. NC mimic + DMSO group; ###P < 0.001 vs. miR-326 mimic + DMSO group, two-way ANOVA with Sidák's post-hoc test.); (F) ELISA was performed to detect the concentrations of IL-6, TNF-α, IL-10, and IL-17 in the culture supernatants of SGC-7901 cells transfected with miR-326 mimic and treated with DMSO or LY294002 (20 μM) for 48 hours. Data are presented as mean ± SD, n = 3 independent experiments with 3 replicates per group. (**P < 0.01 vs. DMSO control group, paired t-test.)

Additionally, this study found that miR-326 regulates the secretion of inflammatory factors, while previous studies did not report similar findings. This may be because this study first measured cytokine levels in cell culture supernatants, thereby capturing the influence of the miR-326/ETS1 axis on the secretion phenotype.

This study found that miR-326 regulates the secretion of cytokines, including IL-6, TNF-α, IL-10, and IL-17, by gastric cancer cells. This finding is consistent with the reports in the literature regarding the regulation of inflammatory responses by the PI3K/Akt pathway (Feng *et al*., 2025). However, it is particularly important to note that all the experiments in this study were conducted only in gastric cancer cell lines and did not involve immune cells or immune co-culture systems. Therefore, the results of this study indicate only that the miR-326/ETS1 axis regulates cytokine secretion in gastric cancer epithelial cells, and cannot be directly inferred to Th17 cell differentiation or more extensive immune regulatory processes. Regarding the role of miR-326 in the tumor immune microenvironment, further verification is needed through experiments such as immune cell co-culture, animal models and clinical immunohistochemical analysis.

CONCLUSION

In conclusion, miR-326 is upregulated in gastric cancer, with significantly elevated expression levels in both gastric cancer tissues and plasma. It is also highly expressed in three gastric cancer cell lines: SGC-7901, MKN-45 and AGS. ETS1 is the direct target gene of miR-326. The dual-luciferase reporter assay confirmed that miR-326 directly binds to the 3'UTR of ETS1 mRNA. Western blot and qRT-PCR showed that miR-326 negatively regulates ETS1 expression. miR-326 activates the PI3K/Akt pathway by targeting ETS1 and overexpression of miR-326 can upregulate the levels of p-PI3K and p-AKT, while co-overexpression of ETS1 can completely reverse this effect. miR-326 promotes the malignant phenotype of gastric cancer cells, and its overexpression significantly enhances proliferation, migration, and invasion, and inhibits apoptosis. Co-overexpression of ETS1 or PI3K inhibitor LY294002 can partially reverse these effects. miR-326 induces an imbalance in inflammatory factors and its overexpression promotes the secretion of pro-inflammatory factors and inhibits the secretion of anti-inflammatory factors. This effect can also be reversed by co-overexpression of ETS1 or LY294002 treatment.

However, the sample size of this clinical study is small and an independent validation cohort is lacking. Therefore, the results of the clinical part should be regarded as preliminary observations and need to be verified in a larger independent cohort. In addition, all functional experiments were conducted only *in vitro using cell lines and lacked validation in animal models in vivo, which cannot assess the overall effect of miR-326 on tumor growth, metastasis,* and the tumor microenvironment. Although the causal relationship was established using the PI3K inhibitor LY294002, genetic validation of key molecules in the PI3K/Akt pathway was not performed using gene knockout or RNA interference. Moreover, the reversal effect of LY294002 was approximately 50%-60%, suggesting the involvement of parallel pathways, which were not explored in this study. This study first revealed the role of the miR-326/ETS1/PI3K/Akt/inflammatory factor regulatory axis in the malignant phenotype of gastric cancer cells, providing a new molecular mechanism for understanding miR-326's function in gastric cancer. These findings suggest that miR-326 and ETS1 may be potential targets for the diagnosis or treatment of gastric cancer, but the application prospects of these targets need to be further verified through animal experiments, clinical cohort studies, and functional rescue experiments.

Acknowledgments
The authors thank the staff of the Sir Run Run Shaw Hospital, School of Medicine, Zhejiang University, for their assistance in sample collection and clinical data organization. Gratitude is also extended to the Laboratory Animal Center and the Cell Biology Core Facility at Sir Run Run Shaw Hospital for providing technical support and access to equipment.

Author's contributions
Kai Liang conceived and designed the study and performed the experiments and acquired the data.
Xiangyu Zhang analyzed and interpreted the data and drafted the manuscript.
Yin Yang revised the manuscript critically for important intellectual content. Supervised the study and provided administrative support.
All authors read and approved the final manuscript and agreed to be accountable for all aspects of the work.

Funding
No Funding was received for this research.

Data availability statement
The datasets generated during and/or analysed during the current study are available from the corresponding author on reasonable request.

Ethical approval
This study was approved by the Ethics Committee of Sir Run Run Shaw Hospital (Approval Number: 202601205). This study was performed in adherence with the STROBE guidelines. See supplementary file for the STROBE checklist.

Conflicts of interest
There are no conflicts to declare.

Supplementary data
https://pjps.pk/uploads/2026/08/SUP1787718732.pdf

REFERENCES

Asensio Lopez MdC, Ruiz Ballester M, Bastida Nicolas FJ, Soler Pardo F, Alonso-Romero JL, Caro-Martinez C, Pascual Figal D and Lax A (2025). miR-106b-5p as a central regulator of cancer progression and chemotherapy-induced cardiotoxicity: From molecular mechanisms to clinical translation. *Int. J. Mol. Sci*., **26**(20): 10002.

Bataga SM, Grama P, Pantea M, Frandes S and Ciurea NA (2026). Prevention of gastric cancer. *Medicina*., **62**(4): 660.

Deng C, Sun S, Zhang H, Liu S, Xu X, Hu Y, Ma H and Xin P (2024). Sappanone A attenuates rheumatoid arthritis via inhibiting PI3K/AKT/NF-κB and JAK2/STAT3 signaling pathways *in-vivo* and *in-vitro*. *Int. Immunopharmacol*., **143**(Pt 3): 113560.

Farc O, Budisan L, Zaharie F, Ţăulean R, Vălean D, Talvan E, Neagoe IB, Zănoagă O, Braicu C and Cristea V (2024). Expression and functional analysis of immuno-micro-RNAs mir-146a and mir-326 in colorectal cancer. *Curr. Issues Mol. Biol*., **46**(7): 7065–7085.

Feng Q, Yu X, Xie J, Liu F, Zhang X, Li S, Wang Y, Pan S, Liu D and Liu Z (2025). Phillygenin improves diabetic nephropathy by inhibiting inflammation and apoptosis via regulating TLR4/MyD88/NF-κB and PI3K/AKT/GSK3β signaling pathways. *Phytomedicine*., **136**: 156314.

Han L, Chen S, Luan Z, Fan M, Wang Y, Sun G and Dai G (2023). Immune function of colon cancer associated miRNA and target genes. *Front. Immunol*., **14**: 1203070.

Han J, Li S, Cao J, Han H, Lu B, Wen T and Bian W (2024). SLC9A2, suppressing by the transcription suppressor ETS1, restrains growth and invasion of osteosarcoma via inhibition of aerobic glycolysis. *Environ. Toxicol*., **39**(1): 238-251.

He F, Wang QF, Li L, Yu C, Liu CZ, Wei WC, Chen LP and Li HY (2023). melatonin protects against hyperoxia-induced apoptosis in alveolar epithelial type II cells by activating the MT2/PI3K/AKT/ETS1 signaling pathway. *Lung*., **201**(2): 225-234.

Hou C, Wu X, Shi R, Xing X, Tian S, Eleouet M, Qiao C, Ma J and Xu G (2024). Subtle structural alteration in indisulam switches the molecular mechanisms for the inhibitory effect on the migration of gastric cancer cells. *Biomed. Pharmacother*., **172**: 116259.

Janjigian YY, Shitara K, Ajani JA, Shen L, Garrido M, Gallardo C, Wyrwicz L, Yamaguchi K, Cleary JM, Elimova E, Bruges R, Karamouzis M, Skoczylas T, Bragagnoli A, Liu T, Tehfe M, Zander T, Kowalyszyn R, Pazo-Cid R, Schenker M and Moehler M (2026). Nivolumab plus chemotherapy as first-line treatment for advanced gastric, gastroesophageal junction and esophageal adenocarcinoma: 5-year follow-up results from CheckMate 649. *Ann. Oncol*., **37**: 787–797.

Ji Y, Wang L, Chang G, Yan J, Dai L, Ji Z, Liu J, He M, Xu H and Zhang L (2023). Mir-421 and mir-550a-1 are potential prognostic markers in esophageal adenocarcinoma. *Biol. Direct*., **18**(1): 5.

Jiang L, Guo F, Tang J, Yu H, Ness S, Duan M, Mao P, Zhao YY and Guo Y (2022). SBSA: an online service for somatic binding sequence annotation. *Nucleic. Acids Res*., **50**(1): e4.

Kadioglu DB, Demirtas CO, Pirim D, Dilber F and Eren F (2024). The preliminary data of gene expressions and bioinformatics analysis of miR-146b-5p and miR-4510 in the Turkish population in HBV-related hepatocellular carcinoma. *Hepatol. Forum*., **5**(3): 106-112.

Li T, Zhang L, Wang P, Yu J, Zhong J, Tang Q, Zhu T, Chen K, Li F, Hong P, Wei J, Sun X, Ji G, Song B and Zhu J (2024). Extracellular vesicles from neural stem cells safeguard neurons in intracerebral hemorrhage by suppressing reactive astrocyte neurotoxicity. *Cell Rep*., **43**(10): 114854.

Liu Y, Zhang L, Wang J, Xu J, Xu J, Xie M and Wang R (2025). Lung cancer cell derived sEVs enhance the metastasis of non-small cell lung cancer via SNHG12/miR-326/SLC7A11 axis. *Cancer Biol. Ther*., **26**(1): 2510041.

Liu Y, Shen L, Li Y, Sun X, Liang L, Jiang S, Zhang Z, Tang X, Tao Y, Xie L, Jiang Y and Cong L (2024). ETS1-mediated regulation of SOAT1 enhances the malignant phenotype of oral squamous cell carcinoma and induces tumor-associated macrophages M2-like polarization. *Int. J. Biol. Sci*., **20**(9): 3372-3392.

Ma X, Wang G, Fan H, Li Z, Chen W, Xiao J, Ni P, Liu K, Shen K, Wang Y, Xu Z and Yang L (2022). Long noncoding RNA FAM225A promotes the malignant progression of gastric cancer through the miR-326/PADI2 axis. *Cell Death Discov*., **8**(1): 20.

Miao Z, Li J, Wang Y, Shi M, Gu X, Zhang X, Wei F, Tang X, Zheng L and Xing Y (2023). Hsa_circ_0136666 stimulates gastric cancer progression and tumor immune escape by regulating the miR-375/PRKDC Axis and PD-L1 phosphorylation. *Mol Cancer*., **22**(1): 205.

Mu G, Li K, Hu C, Cai J, Ruan H, Zhu G and Liu D (2026). GPR176 enhances the epithelial-mesenchymal transition in gastric cancer cells by activating the PI3K/AKT/mTOR signaling pathway. *Oncol. Rep*., **55**(3): 48.

Nafari M, Asri N, Rostami-Nejad M, Forouzesh F, Ehsani-Ardakani MJ, Jahani-Sherafat S, Rezaei-Tavirani M and Aghdaei HA (2022). Elevated interleukin-17A levels despite reduced microRNA-326 gene expression in celiac disease patients under gluten-free diet. *Rom. J. Intern. Med*., **60**(3): 166–172.

Qin X, Jiang Z, Zhu Y, Xue H and Wei C (2022). Long noncoding RNA TMEM147-AS1 serves as a microRNA-326 sponge to aggravate the malignancy of gastric cancer by upregulating SMAD5. *Oncol. Res*.,

29(4): 263-273.

Shen M, Mao Y, Wang X, Huang J, Zhang Q and Zhang J (2024). LncRNA DNM1P35 sponges hsa-mir-326 to promote ovarian cancer progression. *Sci. Rep*., **14**(1): 31502.

Wang M, Jin XE, Xue CM, Liao QB, Pu YF, Liu GQ, Zhuang ZW, Wang YX, Ding Q and Yang XJ (2025a). MiR-155-5p facilitates acute lung injury progression via Th17 cells through the ETS-1/STAT3 pathway. *Gene,* **963**: 149605.

Wang J, Zi F, Liu W, Liu C, Zhang Z, Kong L, Xu X, Wei J, Chen T and Li J (2026). Clostridium butyricum alleviates multiple myeloma by remodeling the bone marrow microenvironment and inhibiting PI3K/AKT pathway through the gut–bone axis. *Gut Microbes*., **18**(1): 2609455.

Wang Y, Gan X, Cheng X, Jia Y, Wang G, Tang X, Du H, Li X, Liu X, Xing X, Ji J and Li Z (2024a). ABCC2 induces metabolic vulnerability and cellular ferroptosis via enhanced glutathione efflux in gastric cancer. *Clin. Transl. Med*., **14**(8): e1754.

Wang L, Li S, Luo H, Lu Q and Yu S (2022). PCSK9 promotes the progression and metastasis of colon cancer cells through regulation of EMT and PI3K/AKT signaling in tumor cells and phenotypic polarization of macrophages. *J. Exp. Clin. Cancer Res*., **41**(1): 303.

Wang FH, Zhang XT, Tang L, Wu Q, Cai MY, Li YF, Qu XJ, Qiu H, Zhang YJ, Ying JE, Zhang J, Sun LY, Lin RB, Wang C, Liu H, Qiu MZ, Guan WL, Rao SX, Ji JF, Xin Y and Xu RH (2024b). The Chinese society of clinical oncology (CSCO): Clinical guidelines for the diagnosis and treatment of gastric cancer, 2023. *Cancer Commun*., **44**: 127–172.

Wang S, Wan L, Zhang X, Fang H, Zhang M, Li F and Yan D (2025b). ETS-1 in tumor immunology: Implications for novel anti-cancer strategies. *Front. Immunol*., **16**: 1526368.

Xiao J, Cao S, Wang J, Li P, Cheng Q, Zhou X, Dong J, Li Y, Zhao X, Xu Z and Yang L (2024). Leptin-mediated suppression of lipoprotein lipase cleavage enhances lipid uptake and facilitates lymph node metastasis in gastric cancer. *Cancer Commun*., **44**(8): 855-878.

Xu X, Zhang L, Ye G, Shi J, Peng Y, Xin F, Lin Y, Wu Q, Lin X and Chen W (2023). Hepatitis B doubly spliced protein (HBDSP) promotes hepatocellular carcinoma cell apoptosis via ETS1/GATA2/YY1-mediated p53 transcription. *J. Virol*., **97**(11): e0108723.

Yang WJ, Zhao HP, Yu Y, Wang JH, Guo L, Liu JY, Pu J and Lv J (2023). Updates on global epidemiology, risk and prognostic factors of gastric cancer. *World J. Gastroenterol*., **29**(16): 2452-2468.

Ye H, Wu Y, Tran R and Wang J (2025). Text mining strategy identifies gene networks under control of miR-21 in breast cancer development. *Cancer Med*., **14**(13): e70986.

Yu JR, Liu YY, Gao YY, Qian LH, Qiu JL, Wang PP and Zhang GJ (2024). Diterpenoid tanshinones inhibit gastric cancer angiogenesis through the PI3K/Akt/mTOR signaling pathway. *J. Ethnopharmacol*., **324**: 117791.

Zhang ZM, Liu ZH, Nie Q, Zhang XM, Yang LQ, Wang C, Yang LL and Song GY (2022). Metformin improves high-fat diet-induced insulin resistance in mice by downregulating the expression of long noncoding RNA NONMMUT031874.2. *Exp. Ther. Med*., **23**(5): 332.